Supporting Information

Vlachos et al. 10.1073/pnas.1213677110

SI Materials and Methods

Thy1-GFP/SP × SP-Deficient Mice. A plasmid containing the ORF of mouse brain synaptopodin (SP) (NM_001109975) fused to the 3′ end of GFP was generously provided by Peter Mundel (Harvard Medical School, Charlestown, MA) (1). For neuron-specific expression the GFP-SP sequence was excised using Eco47III and SmaI and ligated into the blunted XhoI site of pThy1.2 [generously provided by Pico Caroni (Friedrich Miescher Institute for Biomedical Research, Basel, Switzerland) (2)]. The Thy1.2-GFP/SP expression cassette was excised with NotI and PvuI (Fig. S2*A*) and injected into mouse (C57BL/6) pronuclei. Transgenic founder animals were identified by standard PCR of tail tip DNA (forward primer TTTTGCCCTCTGCCCTCTGTTCTC; reverse primer TTGATGCCGTTCTTCTGCTTGTCG; Fig. S2*B*). Transgenic strains were bred by mating transgenic mice to nontransgenic C57BL/6 animals. One of the established Thy1-GFP/SP strains was crossed to SP-deficient mice to obtain mice that lack endogenous SP and express only GFP-SP (Fig. S2*C*).

Thy1-GFP/SP × SP-deficient mice appeared phenotypically normal and showed no obvious alteration in development and fertility. A widespread expression of GFP-SP was detected in hippocampal and other cortical areas in sagittal brain slices of these animals (Fig. S2*D*). In subcortical regions and in the brainstem expression was comparatively low. In the cerebellum GFP-SP was barely seen. In some cortical regions of adult transgenic mice, including some layers of the hippocampus, larger GFP-SP aggregates were found. However, in the 3-wk-old slice cultures no significant difference in mean cluster size of GFP-SP clusters and immunostained SP clusters of wild-type cultures was observed. Immunostainings for SP revealed colocalization of GFP-SP and immunostained SP in Thy1-GFP/SP × SP-deficient mice (Fig. S2*E*; specificity of antibody tested in tissue from SP-deficient mice, Fig. S2*F*), thus confirming that SP clusters are detected in these animals by GFP fluorescence.

Fluorescent Recovery After Photobleaching Analysis. Fluorescent recovery after photobleaching (FRAP) was performed at a Zeiss LSM Exciter confocal microscope at 35 °C as previously described (3). Individual GFP-SP clusters in the molecular layer of the dentate gyrus were visualized using a 40× water immersion objective lens (0.8 N.A.; Zeiss) and 2× scan zoom, with the pinhole diameter set at 1 Airy unit. Image stacks (seven sections) were taken at ideal Nyquest rate. Parameters were initially optimized to minimize bleaching by the imaging procedure itself. Following 15-min baseline registration, selected GFP-SP clusters were completely bleached (<5% of initial fluorescence) using the bleaching function of Zeiss Zen Software (AOTF-controlled Argon laser 488 nm; 100% transmission; 100 bleach iterations) and FRAP followed for 80 min ($\Delta T = 5$ min).

FRAP of individual GFP-SP clusters was corrected for background and bleaching by the imaging procedure itself. Values were normalized to prebleach fluorescence and to the first time point after bleaching. Values were expressed as percentage of mean prebleach fluorescence (i.e., averaged corrected fluorescence of baseline recordings). FRAP data were fitted using the curve fitting toolbox of MATLAB version 7.5 (MathWorks Inc.) with the following biexponential equation:

$$f(t) = P_f \bullet \left(1 - e^{-\frac{t}{\tau_f}}\right) + P_s \bullet \left(1 - e^{-\frac{t}{\tau_s}}\right),$$

where P_f denotes the fraction of the fast component with the recovery time constant τ_f and P_s the fraction of the slow component with the recovery time τ_s. Where appropriate, the fractional contributions of the fast and slow components ($P_{f\text{-}norm}$ and $P_{s\text{-}norm}$, expressed as percentage of the total), the corresponding recovery time constants, as well as the stationary fraction [$1 - (P_f + P_s)$, expressed as percentage] were determined and statistically compared. Owing to difficulties in reliably determining the often rather comparatively small P_f values statistical evaluations were based on comparisons of the averaged FRAP values sampled between 65–80 min per cluster.

When the FRAP curves presented in Fig. 3*C* were fitted using biexponential functions, two kinetically distinct components could be distinguished, a fast one with a recovery time constant of about 10–20 min (τ_f of 11.7 ± 4.0 min in controls and 19.9 ± 16 min after denervation; $P = 0.64$) and a slower one with a constant ranging between 2–4 h (τ_s of 167 ± 48 min in controls and 213 ± 48 min after denervation; $P = 0.34$). Notably, although the τ_f and τ_s values were not significantly different, the relative contributions of the fast and slow components differed significantly in that the relative fraction of the fast component was lower ($P_{f\text{-}norm}$ of 31 ± 4.1% in controls and 13 ± 3.9% after denervation; $P < 0.01$) and of the slow component larger ($P_{s\text{-}norm}$ of 69 ± 4.1% in controls and 87 ± 3.9% after denervation; $P < 0.01$) following denervation compared with controls. The respective stationary fractions were not changed after denervation (22 ± 10% in controls and 17 ± 12% after denervation; $P = 0.75$). These data reveal that reincorporation of GFP-SP into individual clusters is slowed following entorhinal denervation.

Transmission Electron Microscopy. Slice cultures were fixed for 1.5 h in 0.1 M sodium cacodylate buffer (CB) containing 4% (wt/vol) paraformaldehyde, 4% (wt/vol) glutaraldehyde, 15% (vol/vol) picric acid, and 4% (wt/vol) sucrose. After several washes in 0.1 M CB, slices were osmicated (30 min; 1% OsO_4 in 0.1 M CB), dehydrated [60 min; 1% uranyl acetate and 70% (vol/vol) ethanol in H_2O], and embedded between liquid-release-coated slides and coverslips. Slice cultures were reembedded in Durcupan blocks (Fluka) for ultrathin sectioning. Sections were collected on single-slot Formvar-coated copper grids and examined using a Zeiss electron microscope (Zeiss EM 900) by an independent investigator blind to experimental condition. In each culture 20–30 spine apparatuses (SAs; 4–8) were examined in the outer molecular layer and the inner molecular layer of the dentate gyrus at 20,000× magnification and the number of dense plates and endoplasmic cisternae were noted.

Laser Capture Microdissection of Resliced Cultures. Slice cultures were washed with PBS, shock-frozen at −80 °C in tissue-freezing medium (Leica Microsystems), resliced into 10-μm-thick slices on a cryostat (CM 3050 S; Leica), and mounted on PET foil metal frames (Leica). Resliced cultures were fixed in ice-cold acetone for 1 min and incubated with 0.1% toluidine blue (Merck) at room temperature for 1 min before rinsing in ultrapure water (DNase/RNase free; Invitrogen) and 70% (vol/vol) ethanol. PET foil metal frames were mounted on a Leica AS LMD system (Leica Microsystems) with the section facing downward (9). After adjusting intensity, aperture, and cutting velocity, the pulsed UV laser beam was carefully directed along the borders of the granule cell layer (Fig. S5*A*). Tissue from the granule cell layer of the suprapyramidal blade of the dentate gyrus was collected (Fig. S5*A*); that is the area in which granule cells were studied (10, 11). The area of the dissected tissue was determined (Leica Laser Microdissection 6000 System, software version 6.6.3.3564) and tissue areas of approximately equal size (~300×10^3 μm^2) were

harvested from each slice. Microdissected tissue was transferred by gravity into microcentrifuge tube caps placed underneath the sections, filled with 50 μL of guanidine isothiocyanate -containing buffer (RLT Buffer, RNeasy Mini Kit; Qiagen) with 1% β-mercaptoethanol (Appli Chem GmbH). Successful tissue collection was verified by visually inspecting the content of the tube caps. All samples were frozen and stored at −80 °C.

Isolating RNA and Quantitative PCR. RNA was isolated using the RNeasy Micro Plus Kit (Qiagen). Purified RNA was transcribed into cDNA with a High Capacity cDNA Reverse Transcription Kit (Applied Biosystems). All kits and assays were used according to the manufacturer's instructions. The cDNA was amplified using the TaqMan PreAmp Master Mix Kit (Applied Biosystems) using 5 μL of PreAmp Master Mix (Applied Biosystems) + 2.5 μL of cDNA + 2.5 μL of Assay Mix (TaqMan Gene Expression Assays from Applied Biosystems; GAPDH, assay 4352932E; Synaptopodin, assay by design: forward primer, GTCTCCTCGAGCCAAGCA; reverse primer, CACACCTGGGCCTCGAT; probe, TCTCCACCCGGAATGC) with a standard amplification protocol (14 cycles of 95 °C for 15 s and 60 °C for 4 min). Amplified cDNAs were diluted 1:20 in ultrapure water and subjected to quantitative PCR (StepOnePlus; Applied Biosystems) using a standard amplification program (1 cycle of 50 °C for 2 min, 1 cycle of 95 °C for 10 min, 40 cycles of 95 °C for 15 s and 60 °C for 60 s; cut off at 36 cycles).

1. Asanuma K, et al. (2005) Synaptopodin regulates the actin-bundling activity of alpha-actinin in an isoform-specific manner. *J Clin Invest* 115(5):1188–1198.
2. Caroni P (1997) Overexpression of growth-associated proteins in the neurons of adult transgenic mice. *J Neurosci Methods* 71(1):3–9.
3. Vlachos A, Reddy-Alla S, Papadopoulos T, Deller T, Betz H (2012) Homeostatic regulation of Gephyrin scaffolds and synaptic strength at mature hippocampal GABAergic postsynapses. *Cereb Cortex*, 10.1093/cercor/bhs260.
4. Gray EG (1959) Axo-somatic and axo-dendritic synapses of the cerebral cortex: An electron microscope study. *J Anat* 93:420–433.
5. Spacek J (1985) Three-dimensional analysis of dendritic spines. II. Spine apparatus and other cytoplasmic components. *Anat Embryol (Berl)* 171(2):235–243.
6. Spacek J, Harris KM (1997) Three-dimensional organization of smooth endoplasmic reticulum in hippocampal CA1 dendrites and dendritic spines of the immature and mature rat. *J Neurosci* 17(1):190–203.
7. Deller T, Merten T, Roth SU, Mundel P, Frotscher M (2000) Actin-associated protein synaptopodin in the rat hippocampal formation: localization in the spine neck and close association with the spine apparatus of principal neurons. *J Comp Neurol* 418(2): 164–181.
8. Deller T, et al. (2006) Plasticity of synaptopodin and the spine apparatus organelle in the rat fascia dentata following entorhinal cortex lesion. *J Comp Neurol* 499(3): 471–484.
9. Burbach GJ, Dehn D, Del Turco D, Deller T (2003) Quantification of layer-specific gene expression in the hippocampus: effective use of laser microdissection in combination with quantitative RT-PCR. *J Neurosci Methods* 131(1-2):83–91.
10. Vlachos A, et al. (2012) Entorhinal denervation induces homeostatic synaptic scaling of excitatory postsynapses of dentate granule cells in mouse organotypic slice cultures. *PLoS ONE* 7(3):e32883.
11. Becker D, et al. (2012) Functional and structural properties of dentate granule cells with hilar basal dendrites in mouse entorhino-hippocampal slice cultures. *PLoS ONE* 7(11):e48500.

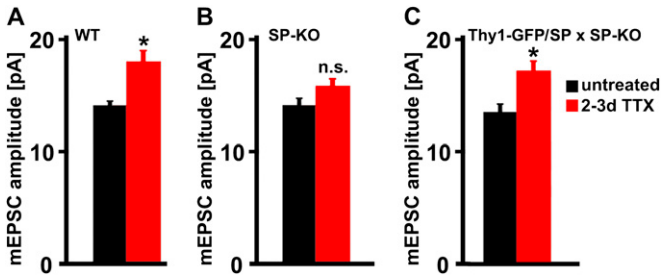

Fig. S1. Tetrodotoxin (TTX)-induced homeostatic synaptic strengthening is impaired in dentate granule cells of SP-deficient entorhino-hippocampal slice cultures. (*A*–*C*) TTX-induced homeostatic synaptic strengthening as seen in (*A*) wild-type cultures is not observed in (*B*) SP-deficient dentate granule cells and can be rescued by expression of (*C*) transgenic GFP-SP (n = 10–13 neurons per group; three to four cultures per group; age- and time-matched control values are also shown in Figs. 1 and 2; Kruskal–Wallis test followed by Dunn's post hoc analysis was used in this study to correct for multiple comparisons). *$P < 0.05$; NS, not significant.

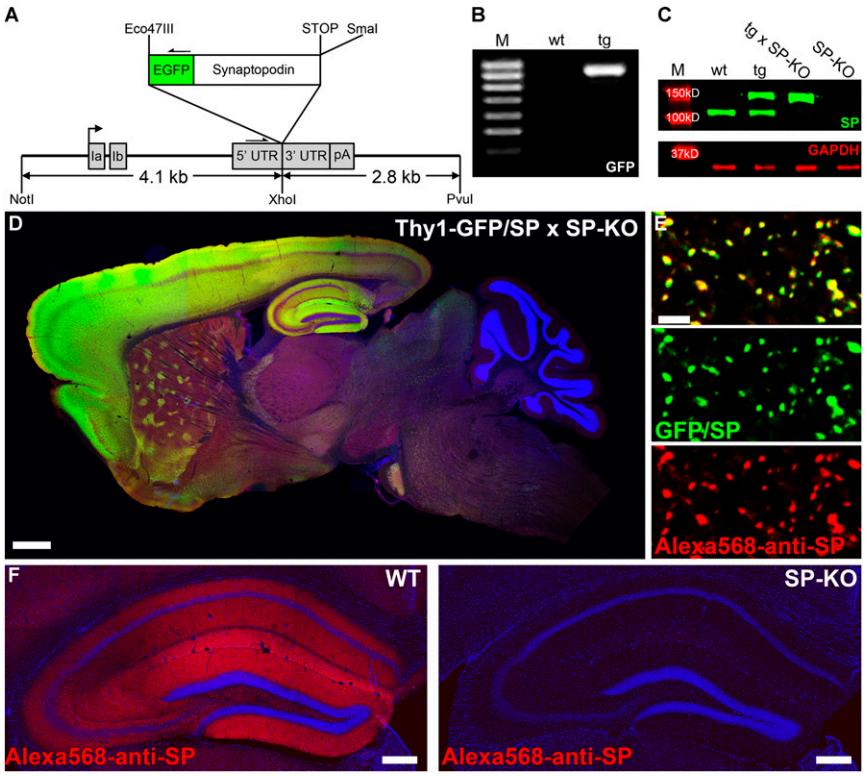

Fig. S2. Generation of Thy1-GFP/SP mice crossed to SP-deficient mice. (*A*) Schematic representation of the construct used to generate transgenic Thy1.2-GFP/SP (Thy1-GFP/SP) mice. A NotI-PvuI fragment of the Thy1.2 expression cassette contains sequences essential for expression. The GFP-tagged mouse SP cDNA was cloned into the XhoI site of the expression cassette. Exons of the Thy1.2 gene are shown as gray boxes. Arrow at exon 1a indicates the transcription start site. pA, polyadenylation sequence; UTR, untranslated region. (*B*) Genotyping from tail DNA by PCR, using a Thy1.2-specific forward primer (Thy1F1) and a GFP-specific reverse primer (GFPrev), reveals a specific 700-bp fragment in Thy1-GFP/SP transgenic (Tg) but not wild-type (WT) mouse (M, DNA marker). (*C*) Thy1-GFP/SP mice were crossed to SP-deficient (SP-KO) animals to obtain a mouse line that lacks endogenous SP and expresses only GFP-SP. Western blot analysis (hippocampal tissue) confirmed that Thy1-GFP/SP × SP-KO mice (tg × SP-KO) express only GFP-SP. (*D*) Sagittal section of Thy1-GFP/SP × SP-KO mouse brain stained for SP (red). Note GFP-SP (green) expression in the hippocampus. Blue, TO-PRO Iodide nuclear stain. (Scale bar: 500 μm.) (*E*) Counterstaining for SP reveals an overlap of immunostained SP clusters (red) and the GFP signal. (Scale bar: 2 μm.) (*F*) Immunostainings for SP in WT and SP-deficient mice disclose the specificity of the antibody (SE-19; Sigma; 1:1,000) used in this study. (Scale bar: 200 μm.)

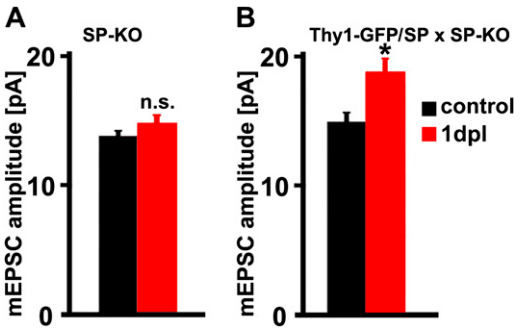

Fig. S3. The early phase of denervation-induced synaptic strengthening requires the presence of SP. (*A* and *B*) Similar to what was observed at 3–4 d post-lesion (dpl), SP-deficient dentate granule cells fail to increase their excitatory synaptic strength at 1 dpl, whereas transgenic expression of GFP-SP rescues the ability of SP-deficient dentate granule cell to show increased miniature excitatory postsynaptic current (mEPSC) amplitudes at 1 dpl ($n = 8–17$ neurons; three to five cultures per group). *$P < 0.05$; NS, not significant.

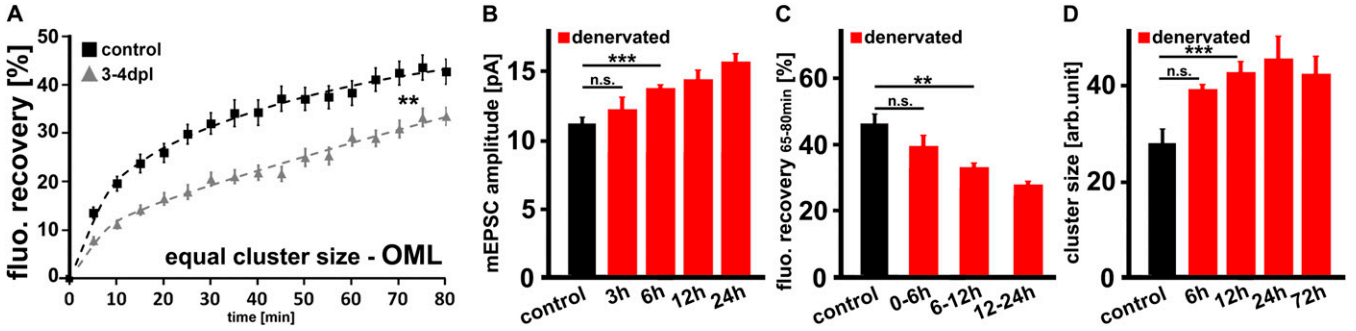

Fig. S4. SP cluster size does not determine fluorescent recovery after photobleaching, but changes in both SP cluster size and stability are linked to the induction of denervation-induced homeostatic synaptic strengthening. (*A*) GFP-SP FRAP of equally sized clusters is decreased after denervation (3–4 dpl) compared with unlesioned controls ($n = 62$ clusters from 12 control cultures; $n = 61$ clusters from 9 denervated cultures; statistical comparison performed with averaged values between 65–80 min per cluster), suggesting that SP cluster size does not determine SP cluster stability. (*B–D*) The compensatory increase in excitatory synaptic strength seen during the first hours following entorhinal denervation in vitro (*B*; data taken from ref. 10) is accompanied by changes in GFP-SP cluster FRAP (C, $n = 24–28$ clusters per group; four cultures each; statistical comparison performed with averaged values between 65–80 min per cluster) and SP cluster sizes (*D*, $n = 4–6$ cultures per group; three to six visual fields per culture). $^{**}P < 0.01$; $^{***}P < 0.001$; NS, not significant.

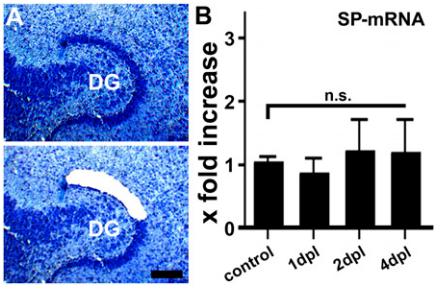

Fig. S5. SP-mRNA levels in the granule cell layer are not changed following entorhinal denervation in vitro. (*A*) It has been previously shown that mRNA levels of SP can increase following the induction of synaptic plasticity (i.e., after LTP-induction) (1, 2). Therefore, we tested whether denervation-induced changes in SP cluster properties correlate with changes in SP mRNA levels. Because SP mRNA is strongly expressed in the granule cell layer (e.g., refs. 1, 3, 4), we harvested tissue from this cell layer from denervated cultures at 1, 2, and 4 dpl as well as from age-matched nondenervated cultures using laser capture microdissection. Tissue from the suprapyramidal blade of the granule cells layer was isolated; that is the area in which all experiments of the present study were performed. Nissl-stained organotypic slice culture. (Scale bar: 100 μm.) (*B*) No significant difference in SP mRNA levels between denervated and age-matched control cultures was observed in this set of experiments ($n = 5$ cultures per group). NS, not significant.

1. Okubo-Suzuki R, Okada D, Sekiguchi M, Inokuchi K (2008) Synaptopodin maintains the neural activity-dependent enlargement of dendritic spines in hippocampal neurons. *Mol Cell Neurosci* 38(2):266–276.
2. Yamazaki M, Matsuo R, Fukazawa Y, Ozawa F, Inokuchi K (2001) Regulated expression of an actin-associated protein, synaptopodin, during long-term potentiation. *J Neurochem* 79(1): 192–199.
3. Mundel P, et al. (1997) Synaptopodin: an actin-associated protein in telencephalic dendrites and renal podocytes. *J Cell Biol* 139(1):193–204.
4. Bas Orth C, et al. (2005) Lamina-specific distribution of Synaptopodin, an actin-associated molecule essential for the spine apparatus, in identified principal cell dendrites of the mouse hippocampus. *J Comp Neurol* 487(3):227–239.

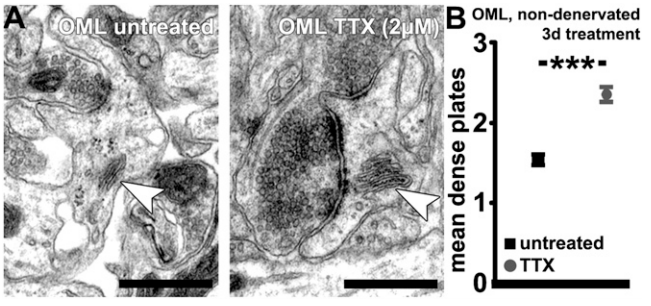

Fig. S6. Effects of prolonged TTX treatment on SA properties in the dentate gyrus of entorhino-hippocampal slice cultures. (*A* and *B*) Similar to denervation, prolonged treatment with TTX (2 μM, 2–3 d) caused an increase in mean dense plate number of SAs ($n = 150$ SAs in five untreated cultures, $n = 218$ SAs in nine TTX-treated cultures; 20–30 SAs per culture). (Scale bar: 0.5 μm.) $^{***}P < 0.001$.